Draft version January 17, 2013
Preprint typeset using LaTeX style emulateapj v. 5/2/11



# DISCOVERY OF X-RAY EMISSION FROM YOUNG SUNS IN THE SMALL MAGELLANIC CLOUD

L. M. Oskinova[1] W. Sun[2], C. J. Evans[3], V. Hénault-Brunet[4], Y.-H. Chu[5], J. S. Gallagher III[6], M. A. Guerrero[7] R. A. Gruendl[5], M. Güdel[8], S. Silich[9], Y. Chen[2], Y. Nazé[10], R. Hainich[1], J. Reyes-Iturbide[11]

*Draft version January 17, 2013*

## ABSTRACT

We report the discovery of extended X-ray emission within the young star cluster NGC 602a in the Wing of the Small Magellanic Cloud (SMC) based on observations obtained with the *Chandra* X-ray Observatory. X-ray emission is detected from the cluster core area with the highest stellar density and from a dusty ridge surrounding the H II region. We use a census of massive stars in the cluster to demonstrate that a cluster wind or wind-blown bubble is unlikely to provide a significant contribution to the X-ray emission detected from the central area of the cluster. We therefore suggest that X-ray emission at the cluster core originates from an ensemble of low- and solar-mass pre-main-sequence (PMS) stars, each of which would be too weak in X-rays to be detected individually. We attribute the X-ray emission from the dusty ridge to the embedded tight cluster of the new-born stars known in this area from infrared studies. Assuming that the levels of X-ray activity in young stars in the low-metallicity environment of NGC 602a are comparable to their Galactic counterparts, then the detected spatial distribution, spectral properties, and level of X-ray emission are largely consistent with those expected from low- and solar-mass PMS stars and young stellar objects (YSOs). This is the first discovery of X-ray emission attributable to PMS stars and YSOs in the SMC, which suggests that the accretion and dynamo processes in young, low-mass objects in the SMC resemble those in the Galaxy.

*Subject headings:* Magellanic Clouds — ISM: bubbles — HII regions — stars: winds, outflows — stars: pre-main sequence — X-rays: stars

## 1. INTRODUCTION

The eastern 'Wing' of the Small Magellanic Cloud (SMC) provides us with an excellent laboratory to investigate the role of environment in star formation and stellar evolution when compared to Galactic studies. The Wing has a low content of gas, dust and stars, with a comparably low metallicity to that found in the main body of the SMC (e.g., Lee et al. 2005). These are typical conditions for low-metallicity dwarf irregular galaxies, which are the most common type among *all* star-forming galaxies (Gallagher & Hunter 1984).

The most significant site of star formation in the Wing is NGC 602, which is a conglomerate of at least three stellar clusters: NGC 602a (immersed in the LHA 115-N 90 H II region, Henize 1956), with NGC 602b adjacent to the north, and NGC 602c ∼11′ to the northeast (Westerlund 1964). Cignoni et al. (2009) advocated a distance modulus to the young stellar population of NGC 602a of 18.7 mag (also see the discussion by Evans et al. 2012); we adopt this distance in the analysis presented here.

The images of NGC 602a from the *Hubble Space Telescope (HST)* Advanced Camera for Surveys (ACS)[12] reveal a star-forming region with a striking ring morphology, as shown in Fig. 1. Massive OB-type stars shine within the broken ring, while lower-mass, pre-main-sequence (PMS) stars are distributed around them (e.g. Carlson et al. 2007; Gouliermis et al. 2007, 2012). Infrared (IR) images from the *Spitzer Space Telescope* show the same morphology, with numerous embedded, young stellar objects (YSOs) revealed in the dusty ridges (e.g. Carlson et al. 2011).

From analysis of the *HST*-ACS and *Spitzer* observations, Cignoni et al. (2009) and Carlson et al. (2011) have argued that the stars in NGC 602a belong to one of three distinct age groups: (i) 6-8 Gyr old very metal-poor field stars; (ii) hot massive stars with ages of a few Myr responsible for the ionization of N 90 and low-mass PMS stars of the same age; (iii) tens of kyr old YSOs (Class 0.5-I) embedded in the dusty ridges and pillars. The cluster mass has been estimated as $\sim 2000\,M_\odot$ (Cignoni et al. 2009; Carlson et al. 2011). The star-formation rate in NGC 602a was determined by Cignoni et al. (2009) to have reached $(0.3 - 0.7) \times$

[1] Institute for Physics and Astronomy, University Potsdam, 14476 Potsdam, Germany
[2] Department of Astronomy, Nanjing University, Nanjing, 210093 Jiangsu, China
[3] UK Astronomy Technology Centre, Royal Observatory Edinburgh, Blackford Hill, Edinburgh, EH9 3HJ, UK
[4] Scottish Universities Physics Alliance (SUPA), Institute for Astronomy, University of Edinburgh, Blackford Hill, Edinburgh EH9 3HJ, UK
[5] Department of Astronomy, University of Illinois, 1002 West Green Street, Urbana, IL 61801, USA
[6] Department of Astronomy, University of Wisconsin-Madison, 5534 Sterling, 475 North Charter Street, Madison, WI 53706, USA
[7] Instituto de Astrofísica de Andalucía, IAA-CSIC, Glorieta de la Astronomía s/n, 18008 Granada, Spain
[8] University of Vienna, Department of Astrophysics, Türkenschanzstrasse 17, 1180, Vienna, Austria
[9] Instituto Nacional de Astrofísica Optica y Electrónica, AP 51, 72000 Puebla, Mexico
[10] GAPHE, Département AGO, Université de Liège, Allée du 6 Août 17, Bat. B5C, B4000 Liège, Belgium
[11] LATO-DCET/Universidade Estadual de Santa Cruz, Rodovia Jorge Amado, km 16, 45662-000 Ilhéus, BA, Brazil

[12] http://hubblesite.org/newscenter/archive/releases/2007/04

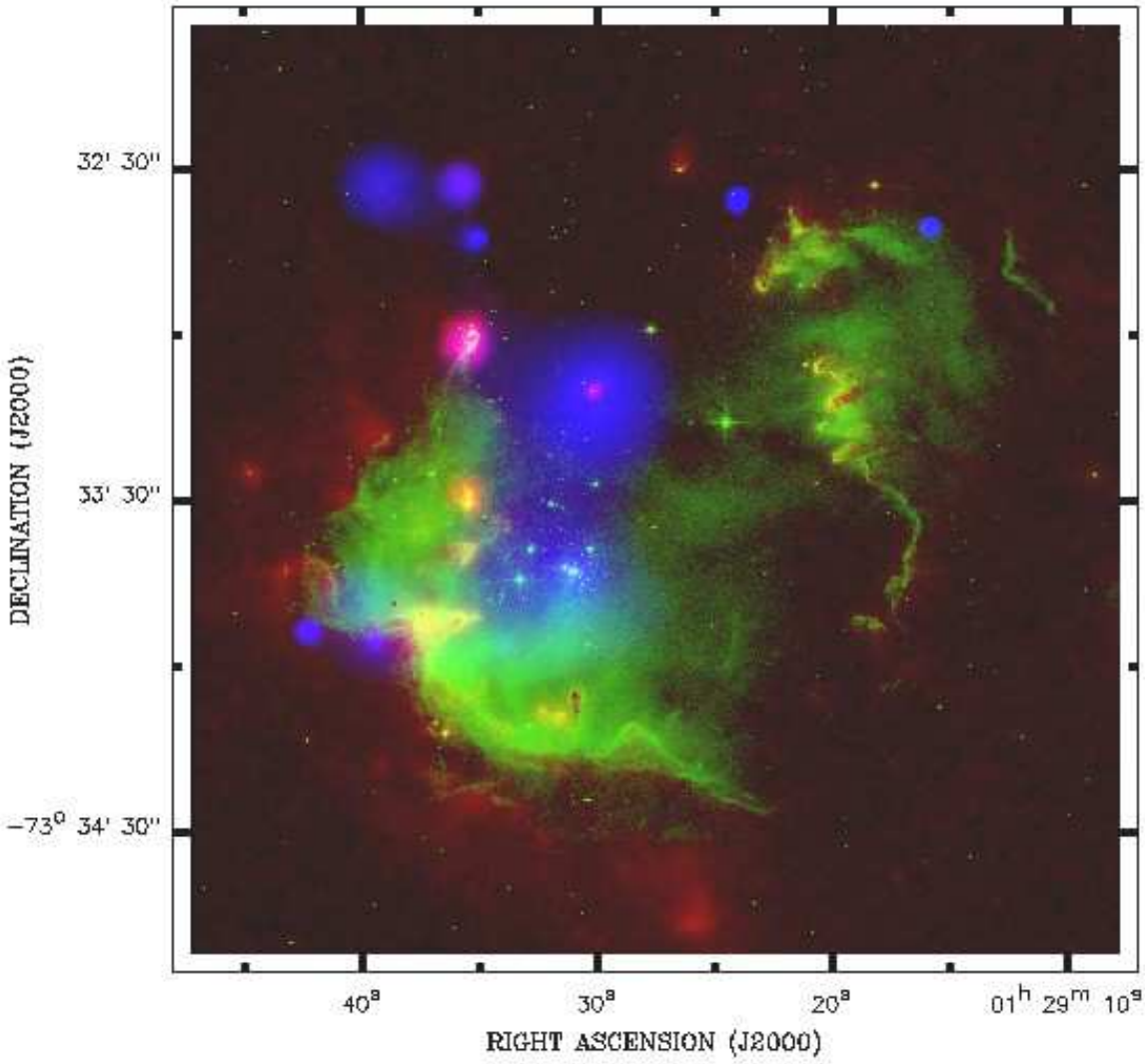


**Figure 1.** Color-composite image of NGC 602a, constructed from observations with *Spitzer*–IRAC at 8 $\mu$m (red, AOR 12485120), *HST*–ACS with the F658N filter (green, data set J92FA6), and *Chandra* ACIS-I in the 0.5-7.0 keV band (adaptively smoothed, in blue). Image size is $\approx 2' \times 2'$ ($\approx 32$ pc$\times$32 pc).

$10^{-3}\,M_\odot\,\mathrm{yr}^{-1}$ in the last 2.5 Myr, comparable to that found in Galactic OB associations.

As part of a combined X-ray–optical study of NGC 602 and its associated H$\alpha$ supergiant shell ('SGS-SMC1', Meaburn 1980) we obtained deep X-ray imaging of NGC 602 with the *Chandra X-ray Observatory*, giving the best opportunity to date to study the SMC's Wing at X-ray wavelengths. This paper presents and discusses these new observations.

In the context of deep X-ray observations, the Orion Nebular Cluster (ONC, M 42) provides a useful Galactic comparison. Indeed, the ONC – located at a distance of ∼0.4 kpc (e.g. Sandstrom et al. 2007) – is one of the best-studied young, massive star clusters. It has a cluster stellar mass of $\approx 1800\,M_\odot$ within 2 pc (Hillenbrand & Hartmann 1998)[13] and contains multiple stellar generations with ages of $0.1 - 3$ Myr, with a lower limit to the recent star-formation rate of $\sim 10^{-4}\,M_\odot\,\mathrm{yr}^{-1}$. The cluster core is compact with a radius $\lesssim$0.5 pc (Hillenbrand 1997; Hillenbrand & Hartmann 1998). Most pertinently, the ONC has been studied extensively in X-rays (e.g., Schulz et al. 2001; Feigelson et al. 2002; Flaccomio et al. 2003; Güdel et al. 2008), with deep *Chandra* observations revealing the X-ray properties of its young stars (see the ApJS special is-

[13] Note that Alves & Bouy (2012) found a rich stellar population in front of the Orion A cloud, in which the ONC is embedded. This 4-5 Myr old cluster (NGC 1980) in front of the ONC is quite massive ($\sim 1\,000 M_\odot$) and overlaps significantly with what is usually assumed to be the ONC. It could account for more than 10-20% of what is taken in the literature as the ONC population.

sue, vol. 160, Getman et al. 2005), which are considered a template for massive star-forming region.

The mass, size, range in stellar ages, and star-formation history of the ONC are comparable to NGC 602a. The stellar initial mass function (IMF) for stars more massive than $1\,M_{\odot}$ in NGC 602a was found by Schmalzl et al. (2008) to be similar to a Salpeter IMF, i.e., comparable to the field IMF in the solar neighbourhood. Albeit there is a difference in the exact number of high-mass stars between the ONC (6 stars, Hillenbrand 1997) vs. NGC 602a (10 stars, Schmalzl et al. 2008), such differences are to be expected from stochastic sampling of the IMF in relatively low-mass star clusters (e.g. Cerviño & Valls-Gabaud 2003).

In accordance with other results found for the SMC clusters (e.g., NGC 346, Massey et al. 1995; Sabbi et al. 2008; De Marchi et al. 2011), this suggests that the star-formation process is similar between the SMC and the Galaxy (e.g. Chabrier 2003). However, it is not yet clear how low metallicity of the SMC affects the physical properties of the stars. In massive stars the wind momentum may be depend on metallicity (e.g. Puls et al. 1996). In young low-mass stars the metallicity effects could lead to different coronal and accretion properties. Additionally, a metal-poor environment might lead to reduced radiative losses from X-rays, thus affecting disk formation. For example, Yasui et al. (2009) suggested that stars forming in a low-metallicity environment experience disk dispersal a few Myr earlier compared to those with solar abundances. The dynamo process which powers X-ray coronae may also be affected by metallicity (e.g. Pizzolato et al. 2001).

There are only very few deep X-ray observations of star-forming regions in environments which are very different to our Galactic neighborhood (e.g. Caramazza et al. 2012). Previous X-ray observations of star-forming regions in the SMC were not sensitive enough to detect the X-ray emission from low- and solar-mass stars (e.g. Nazé et al. 2003). The new *Chandra* data presented here provide us with an opportunity to investigate the X-ray behaviour of young stellar populations in the low metallicity of the SMC for the first time.

In this paper we present the *Chandra* observations, which have revealed extended X-ray emission in NGC 602a. Section 2 presents the observations, data reduction, the detected point-sources and the details of the extended X-ray emission. The X-ray emission from massive stars is considered in Section 3. Section 4 discusses the possible origins of the extended emission, with a summary given in Section 5. In Appendix the details about the X-ray point sources are provided, and the neutral column density towards NGC 602a is deduced.

## 2. OBSERVATIONS AND DATA REDUCTION

The data were obtained with the *Chandra* ACIS-I detector. The observations comprised 11 exposures acquired between 2010 March 31 and 2010 April 29 with an effective exposure time of 290.7 ks. A combined optical, IR and X-ray image of the cluster is shown in Fig. 1.

The *Chandra* data-reduction package CIAO (v4.3) was used for calibration of the X-ray data and extraction of the spectra[14]. Point-like sources were detected in three broad bands ('S': 0.5-2.0 keV, 'H': 2.0-8.0 keV, 'B': 0.5-8.0 keV) using the procedures from Wang (2004).

The detection procedures use a combination of algorithms: wavelet detection, a 'sliding-box' method, and maximum likelihood centroid fitting. The source count rates are estimated from the net counts within the 90% energy-encircled radius determined by the telescope/ACIS point-spread function (PSF, Jerius et al. 2000). The PSFs are different in the soft and hard bands, therefore the point-source detection was undertaken in the individual bands. The detection limit is characterized by a threshold probability (we used $1\times10^{-6}$), which describes the probability of a false detection of a random variation above the background as a point source.

For our observations we used the position-dependent 70% energy-encircled radius as the detection aperture (Jerius et al. 2000), corresponding to $\sim1\farcs2$ (0.3 pc) in NGC 602a. The adopted threshold probability allowed us to detect point sources with a count-rate of $0.05\,\mathrm{cts\,ks^{-1}}$ in a broad band, corresponding to 14 source counts ($3\sigma$ detection). No flaring activity within NGC 602a was detected during our observations.

### 2.1. *Point sources detected in NGC 602a*

Nine point sources were detected within $2'$ ($\sim32$ pc) of the core of NGC 602a. These are summarised in Table 1 and their locations are overlaid on an optical *HST* image in Fig. 2. Source 2 has no optical counterparts within a radius of $1''$ (cf. the source catalogue from Schmalzl et al. 2008); we believe it to be a background source. The counterparts of the remaining sources are discussed in more detail in the Appendix. Two (sources 4 and 5) are located in the dense core of NGC 602a, with source 5 apparently coincident with a late O-type star. Source 3 is a newly-discovered quasar, QSO J012930-733311. Using our own optical spectra obtained with VLT-FLAMES we determined its redshift as $z=2.4$.

We use the X-ray spectral analysis of QSO J012930-733311 to estimate the neutral hydrogen column density towards NGC 602a (see Section A.2). Throughout this paper we use a two component absorption model, with Galactic foreground absorption at $6\times10^{20}\,\mathrm{cm^{-2}}$ (Wilms et al. 2000) and a second component with SMC abundances at $2\times10^{21}\,\mathrm{cm^{-2}}$.

### 2.2. *Extended X-ray emission*

The high angular resolution of *Chandra* allowed us to disentangle bright point sources from areas of extended X-ray emission. After subtraction of the point sources, inspection of the adaptively-smoothed X-ray images reveals apparent areas of extended, diffuse emission in NGC 602a (see Figs. 1 – 4). The largest area of extended emission is centered on the central part of NGC 602a, with a more compact area of emission coincident with the sub-cluster of YSOs Y327 (Carlson et al. 2011). The third area is to the north of the cluster and coincides with a galaxy seen in the *HST* images (see Fig. 2).

Formal detection of extended X-ray emission must satisfy two criteria: (1) the extended emission shall be above the background fluctuations and, (2) it should be truly extended, with a radial profile that is wider than that of

[14] All X-ray spectra discussed here were analyzed using the XPSEC v12 spectral fitting package (Arnaud 1996).

**Table 1**
*Chandra* X-ray Point Sources in NGC 602a

| Src | CXOU Name | $\delta_x$ ($''$) | CR (cnt ks$^{-1}$) | HR | HR1 | Flag | Counterparts |
|---|---|---|---|---|---|---|---|
| (1) | (2) | (3) | (4) | (5) | (6) | (7) | (8) |
| 1 | J012915.85-733240.7 | 0.7 | $0.05 \pm 0.02$ | – | – | B | ? |
| 2 | J012924.03-733236.3 | 0.4 | $0.26 \pm 0.04$ | $0.10 \pm 0.18$ | $1.00 \pm 0.00$ | H,B,S | ? |
| 3 | J012930.17-733310.7 | 0.3 | $15.02 \pm 0.32$ | $-0.26 \pm 0.03$ | $0.42 \pm 0.03$ | B,S,H | QSO J012930-733311 |
| 4 | J012930.98-733344.2 | 0.5 | $0.08 \pm 0.03$ | – | – | S,B | cluster center? |
| 5 | J012931.29-733342.2 | 0.5 | $0.06 \pm 0.02$ | – | – | S | O9.5V star? |
| 6 | J012935.13-733242.8 | 0.4 | $0.18 \pm 0.04$ | $-0.91 \pm 0.18$ | $0.50 \pm 0.19$ | S,B | ? |
| 7 | J012935.79-733233.1 | 0.4 | $0.21 \pm 0.04$ | – | $0.43 \pm 0.19$ | S,B | galaxy 'G372' |
| 8 | J012939.52-733355.3 | 0.5 | $0.25 \pm 0.04$ | $0.08 \pm 0.20$ | $0.75 \pm 0.19$ | B,S,H | ? |
| 9 | J012942.31-733353.5 | 0.5 | $0.17 \pm 0.03$ | – | – | B,S,H | galaxy |

**Note**. — Definition of the *Chandra* bands: 0.5–1 (S1), 1–2 (S2), 2–4 (H1), and 4–8 keV (H2), with S = S1 + S2, H = H1 + H2, and B = S + H. Columns: (1) Generic source number; (2) Adopted *Chandra* identification; (3) Positional uncertainty ($1\sigma$) calculated from the maximum likelihood centroiding error and an approximate off-axis angle ($r$) dependent systematic error: $0\farcs2 + 1\farcs4(r/8')^2$, (an approximation to Fig. 4 from Feigelson et al. 2002), and added in quadrature; (4) On-axis source broad-band count rate (the sum of the exposure-corrected count rates in the four bands); (5, 6) The hardness ratios, defined as HR = (H − S2)/(H + S2), and HR1 = (S2 − S1)/S; (7) 'B', 'S', or 'H' indicates the band in which a source is detected and the source of the quoted position in Col. 2; (8) Information on counterparts, see the Appendix for further details;

the PSF. The first criterion is checked using image contours at the $5\,\sigma$ and $3\,\sigma$ levels (e.g., Fig. 2). Once an area is identified as possible extended emission, its extent is checked by building a radial profile, which is then compared with the profile from a point-like source of similar brightness (see Fig. 5). Gouliermis et al. (2012) showed that NGC 602a is hierarchically structured, and identified sub-clusters that differ in age, mass, and size (their Table 1). Two of the areas of extended X-ray emission coincide with their two most populous sub-clusters (see Fig. 4), which are now discussed in more detail.

#### 2.2.1. *Sub-cluster 1: the core of NGC 602a*

At least seven OB-type stars and numerous lower-mass stars reside in 'sub-cluster 1' (Gouliermis et al. 2012), with the stellar density distribution comparable to the distribution of extended X-ray emission (see Fig. 4). A comparison of the radial profile of the X-ray emission filling the interior of sub-cluster 1 with the ACIS PSF is shown in Fig. 5, demonstrating that the X-ray emission is indeed extended.

After removal of the detected point sources, an X-ray spectrum was extracted from an area of $\approx 18\,\mathrm{pc}^2$ (as shown by the solid circle in Fig. 6). We investigated in detail the effects of the background. The spectra obtained using different background areas are similar, and they are always above the background level. E.g. the total (together with background) count rates (over 0.5-8.0 keV band) of extended X-ray emission from sub-cluster 1 is $(5.0 \pm 1.0) \times 10^{-4}\,\mathrm{counts\,s^{-1}}$, while the ambient background count-rate in the same band is $(0.6 \pm 1.0) \times 10^{-4}\,\mathrm{counts\,s^{-1}}$. Therefore, the source spectrum is about $3\sigma$ above the background spectrum.

To derive the spectral parameters, we first attempted a spectral fit with a two-temperature plasma model. Unfortunately, due to the small number of the spectral counts, the 2-T model parameters could not constrained. Therefore, we use an APEC isothermal plasma model, adopting SMC abundances and the absorption model as obtained from the fits to the nearby, newly-discovered QSO J012930-733311 (see Section A.2). The best fit one-temperature model has $\mathrm{kT} = 2.1 \pm 1.3\,\mathrm{keV}$ with an emission measure of $(10 \pm 3) \times 10^{55}\,\mathrm{cm^{-3}}$, The model observed flux is $2 \times 10^{-15}\,\mathrm{erg\,s^{-1}\,cm^{-2}}$ in the 0.5-8.0 keV and corresponding luminosity of the extended X-ray emission in sub-cluster 1 is $L_\mathrm{X} \approx 1 \times 10^{33} - 2 \times 10^{33}\,\mathrm{erg\,s^{-1}}$.

#### 2.2.2. *Sub-cluster 2: the tip of "elephant trunk"*

Extended X-ray emission (over an area of $\sim 12\,\mathrm{pc}^2$ or $\sim 55\,\mathrm{arcsec}^2$) is also detected from 'sub-cluster 2', the second most populous sub-cluster in the region (Gouliermis et al. 2012). Located at the tip of an 'elephant trunk' associated with star formation and on the northeastern limb of the N 90 H II region, sub-cluster 2 is a good example of a compact cluster at an earlier evolutionary stage than NGC 602a.

Two IR-bright, massive YSOs were identified in 3.6 $\mu$m *Spitzer* images by Gouliermis et al. (2007, their sources 54 and 57). Carlson et al. (2011) collectively refer to these, and other nearby bright sources, as 'Y327' (this label is also used to identify the sub-cluster in Fig. 2) and identified them as Class I YSOs (younger than $\sim 10^5$ yr). Class I YSOs are surrounded by in-falling dusty envelopes, which continue to accrete mass and produce outflows (Adams et al. 1987).

Only 22 counts were detected from the *Chandra* observations of sub-cluster 2, none of which were at energies below 1 keV, confirming that this object is highly embedded. Comparing the number of counts at different radii with those expected from a point source confirms that X-ray emission is extended at this position. It is difficult to estimate the intrinsic luminosity as we do not know the column density and extinction law in this region. Adopting an *ad hoc* $N_\mathrm{H} = 10^{22}\,\mathrm{cm^{-2}}$ with a thermal plasma with temperature $\sim 2\,\mathrm{keV}$ we estimate the *model dependent* X-ray luminosity of sub-cluster 2 to be $L_\mathrm{X} \approx 6 \times 10^{32}\,\mathrm{erg\,s^{-1}}$ in the 0.5-8.0 keV band.

## 3. X-RAY EMISSION FROM MASSIVE STARS IN NGC 602a

On the basis of *HST* photometry, Schmalzl et al. (2008) identified the 10 brightest stars of NGC 602a as massive stars (i.e. with inferred spectral types of B0.5 or earlier). Among all these stars, only the O9.5V star SGD 13 is marginally detected in our observations (see discussion in Section A.4).

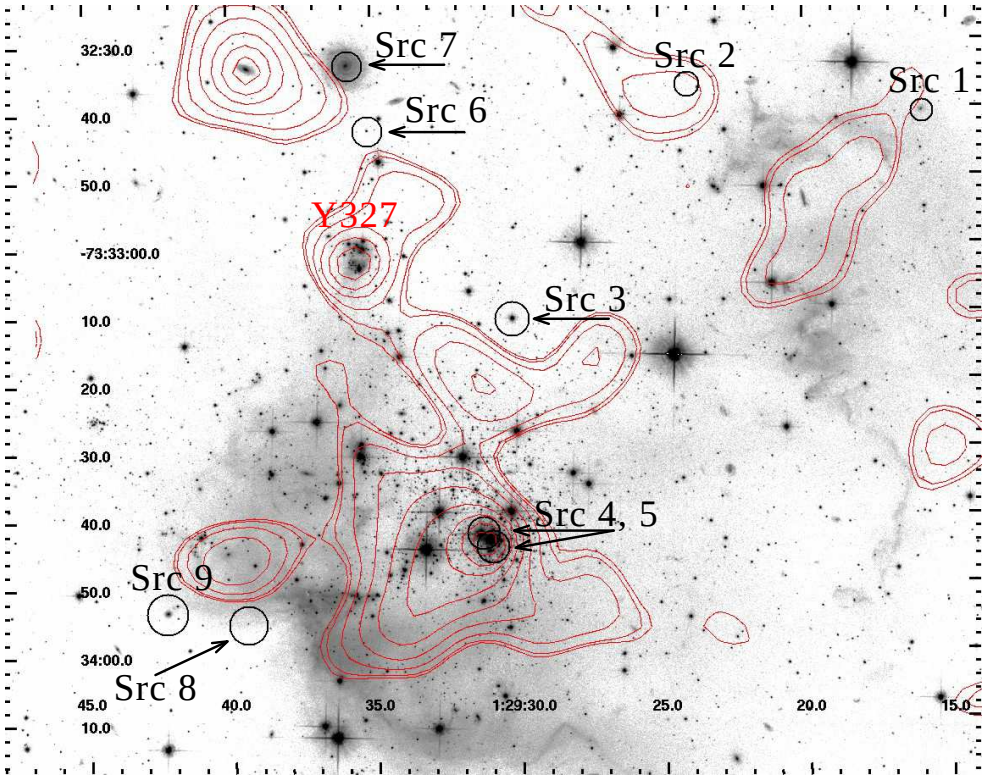


**Figure 2.** *HST* image of NGC 602a (F658N filter, north is at the top, east to the left). Black circles are point sources detected by *Chandra* (Table 1). Red contours show areas of extended X-ray emission at the $3\,\sigma$ level. From north-to-south, the three areas of notable extended X-ray emission correspond to a background spiral galaxy and sub-clusters 2 and 1 from Gouliermis et al. (2012). North is up, and east is to the left.

For Galactic single and binary OB stars the bolometric and X-ray luminosities are seen to correlate as $\log L_{\rm X}/L_{\rm bol} \sim -7$ (e.g. Seward et al. 1979; Pallavicini et al. 1981; Berghoefer et al. 1997; Oskinova 2005; Nazé 2009). X-ray detections of normal massive stars in other galaxies are scarce so it is unknown how this correlation scales with environment. Given that the strength of stellar winds decreases with metallicity (e.g. Puls et al. 1996; Vink et al. 2001; Mokiem et al. 2007; Gräfener & Hamann 2008), we expect that O-type stars in the SMC are less X-ray luminous than in the Galaxy.

To estimate an upper limit to the X-ray luminosity of undetected OB-type stars in NGC 602a, we adopt the line-of-sight neutral hydrogen value from analysis of the nearby QSO X-ray spectrum (Section A.2), and assume that the X-ray spectral model is similar to that found typically in Galactic massive stars, i.e., an optically-thin plasma in collisional equilibrium, characterized by $T \sim 5$ MK. With these assumptions, any massive stars not detected by *Chandra* in NGC 602a should have X-ray luminosities of $\lesssim 1.5 \times 10^{32}\,{\rm erg\,s^{-1}}$. Adopting this limit, if massive stars in the SMC were as X-ray luminous as their Galactic counterparts, then only the most massive stars (with spectral types earlier than O4 V) would have been detected.

Using optical spectroscopy with VLT-FLAMES of massive stars in and around NGC 602a (Hainich et al. in prep.) we found that Sk 183, is the only star in NGC 602a with such an early spectral type. However, it was not detected in our X-ray observations. Given the detection limit calculated above, the maximum X-ray luminosity for Sk 183 (compared to its bolometric luminosity) is $\log L_{\rm X}/L_{\rm bol} \lesssim -7.2$.

After Sk 183, the next most massive stars known in the cluster are late O-type dwarfs (e.g. Hutchings et al. 1991, Hainich et al. in prep.). The X-ray luminosities of Galactic late O-type stars are typically much lower than the detection limit of the *Chandra* observations in NGC 602a. For instance, both $\zeta$ Oph (O9 V) and $\mu$ Col (O9.5 V) have $L_{\rm X} \approx (1.2-1.3) \times 10^{31}\,{\rm erg\,s^{-1}}$ (Oskinova et al. 2001; Huenemoerder et al. 2012); in both cases this corresponds to $\sim 10^{-7}$ of their bolometric luminosity.

The correlation of X-ray to bolometric luminosity can have a spread of up to 1 dex (e.g. Nazé et al. 2011). However, if $L_{\rm X}$ exceeds $10^{-7} L_{\rm bol}$ it strongly indicates that the star is either a colliding-wind binary (e.g. Stevens et al. 1992; Antokhin et al. 2004; Pollock & Corcoran 2006), or has a magnetically-confined wind (e.g. Babel & Montmerle 1997; Donati et al. 2002)[15]. In these cases one would also expect relatively hard X-ray emission (e.g. Gagné et al. 2005; Ignace et al. 2012; Nazé et al. 2012). Even more significant X-ray fluxes would be expected from massive stars with a degenerate (neutron star or black hole) companion, for which $\log L_{\rm X}/L_{\rm bol} \lesssim -4 \ldots -3$ (Liu et al. 2005).

The fraction of binaries among O-type stars is very high (up to 70%), especially in young clusters (Chini et al. 2012; Sana et al. 2012). It is likely, that there are binaries among massive stars in NGC 602a. The non-detection of these stars in X-rays shows that

[15] We note that binary stars and magnetic stars can also exhibit average X-ray luminosities and soft X-ray spectra (Drake et al. 1994; Oskinova 2005; Nazé 2009; Oskinova et al. 2011)

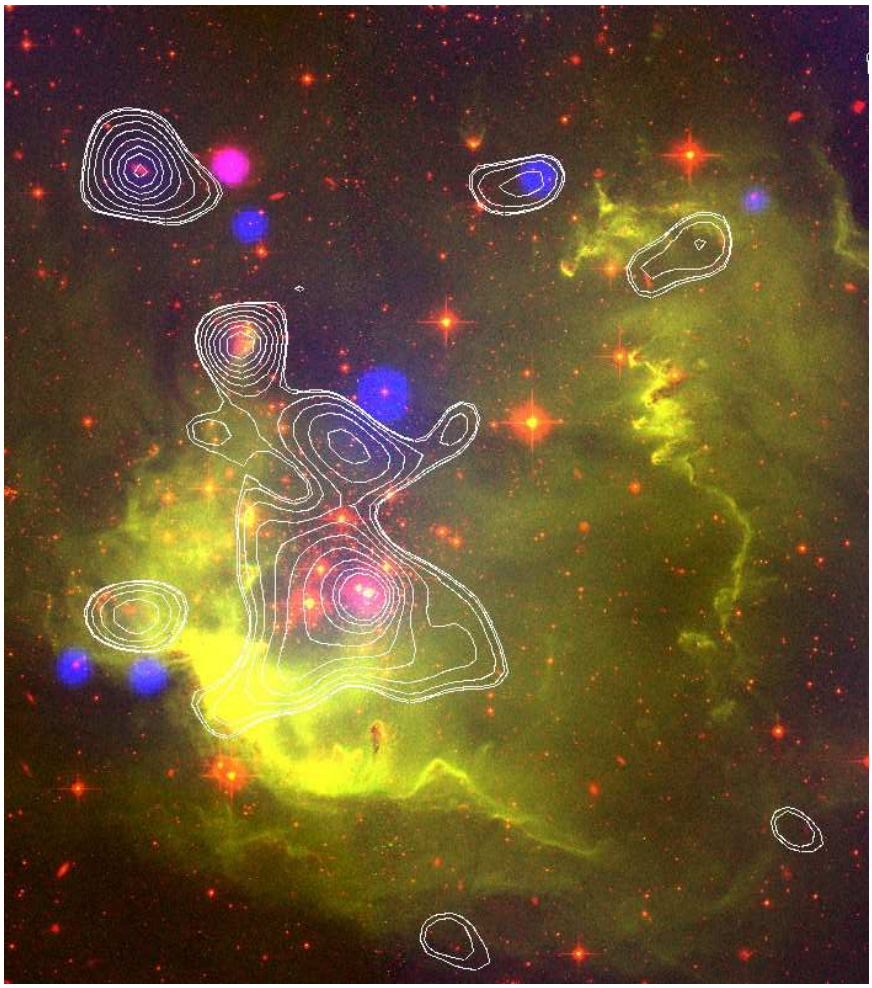

**Figure 3.** Color-composite image of NGC 602a. *HST* images are in red (F814W filter) and green (F658N filter). The blue image is the *Chandra* 0.5-8.0 keV band with X-ray point sources removed and adaptively smoothed. The contours tracing the extended X-ray emission are the same as in the middle panel in Fig. 4. Image size is $\approx 2.6' \times 2.6'$ ($\approx 42\,\mathrm{pc} \times 42\,\mathrm{pc}$). North is up, and east is to the left.

a colliding wind binary phenomenon is quite rare among dwarf O-type stars. This may be due to the weakness of their stellar winds, as X-ray luminosity scales with $\dot{M}^2$ (Stevens et al. 1992). Therefore, the upper limits on X-ray emission from massive stars in NGC 602a are in agreement with expectations.

Given the deep optical and IR imaging available, the census of massive stars in NGC 602 can be assumed to be complete (to first order) and, aside from the notable high X-ray luminosity of source 5 ($L_{\rm X} = 3 \times 10^{32}\,\mathrm{erg\,s^{-1}}$, see discussion in Section A.4), it seems extremely unlikely that the extended emission in sub-cluster 1 could be accounted for by an unresolved/undetected population of high-mass stars.

## 4. ORIGINS OF THE EXTENDED EMISSION

In this section we discuss the origins of the extended X-ray emission detected in sub-clusters 1 and 2.

### 4.1. *Extended Emission from a Wind-blown Bubble?*

The intracluster gas in a stellar cluster can be heated by the mechanical energy input from stellar winds. This can result in an outflow of a hot cluster wind and creation of a wind-blown bubble (WBB). Indeed, the diffuse X-ray emission from hot gas is often observed in star-forming regions (e.g. Townsley et al. 2003; Güdel et al. 2008; Townsley et al. 2011). The density and the temperature of the hot, X-ray emitting gas is largely determined by the kinetic energy input and depends sensitively on the cluster mass, age, and metallicity (Chu & Mac Low 1990; Stevens & Hartwell 2003; Oskinova 2005). Theoretical models from Silich et al. (2005) indicate that the X-ray production efficiency by the diffuse intracluster gas is generally low, with $L_{\rm X}/L_{\rm mech} \ll 1\%$, as found by Smith et al. (2005). In the absence of recent SNe, the heating of the WBB is entirely due to the stellar winds, and is determined by the total number of massive stars and kinetic energy of their winds.

As was already discussed above, ten massive stars in NGC 602a are known – an average number for a cluster of such mass. The most massive star in NGC 602a, Sk 183, is $\sim 45''$ ($\sim 12\,\mathrm{pc}$) to the northwest of sub-cluster 1. The earliest type stars known in sub-cluster 1 are three late O-type dwarfs (see Sections A.3, A.4).

To estimate the combined feedback from stellar winds in this sub-cluster we need to know their mass-loss rates and wind velocities. Mokiem et al. (2006) investigated wind parameters for late O-type stars in the SMC. Their mass-loss rates (in the range of $10^{-7}$ to $10^{-8}\,M_\odot\,\mathrm{yr^{-1}}$) were obtained from analysis of the observed H$\alpha$ pro-

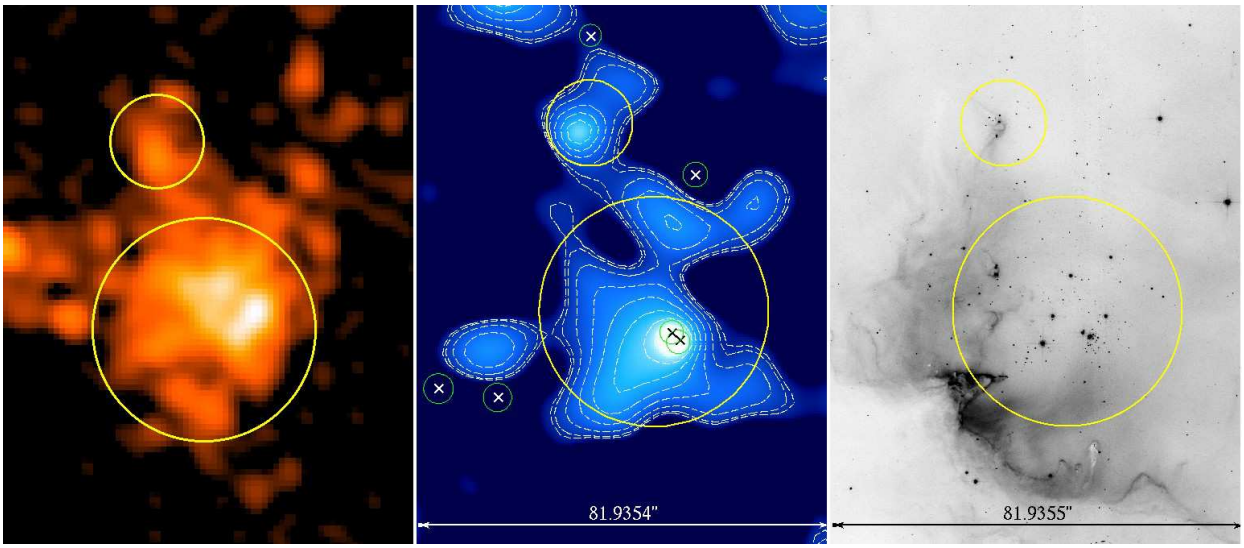


**Figure 4.** *Left panel:* Stellar density map of the low-mass PMS stars in the two most dense sub-clusters in NGC 602a (image courtesy of D. A. Gouliermis, see Figs. 5 & 9 in Gouliermis et al. (2012) for details). *Middle panel:* Adaptively-smoothed *Chandra* image of a part of NGC 602a. White contours trace the extended X-ray emission on a square-root scale, from $5 \times 10^{-4}$ cnt s$^{-1}$ arcmin$^{-2}$ to $8 \times 10^{-4}$ cnt s$^{-1}$ arcmin$^{-2}$. The encircled crosses show point sources detected by *Chandra*, but note that all but these two point sources have been subtracted prior from this image. *Right panel*: *HST* F658N image of the same area for comparison. Sub-clusters 1 and 2 are shown in all three panels by the overlaid yellow circles, with centers and radii from Table 1 of Gouliermis et al. (2012).

files. In late O-dwarfs, H$\alpha$ is in absorption and does not significantly depart from a pure photospheric profile. Combining optical and UV spectroscopy helps to set more stringent limits on mass-loss rates. The UV spectra obtained with *HST* STIS combined with optical spectroscopy were used by Bouret et al. (2003) to analyse O-dwarfs in the SMC. They derived mass-loss rate $1 \times 10^{-10}\,M_\odot\,\mathrm{yr}^{-1}$ and $v_\infty \sim 1000\,\mathrm{km\,s}^{-1}$ for a O9.5V-type star. Similarly, combining optical and UV spectroscopy, Martins et al. (2004) determined that the winds of O-dwarfs in the SMC cluster N 81 (located in the SMC Wing) are weak, with mass-loss rates typically lower than few $\times\, 10^{-9}\,M_\odot\,\mathrm{yr}^{-1}$ and rather low wind velocities. Oskinova et al. (2007) showed that to derive accurate mass-loss rate from UV resonance lines, stellar wind clumping has to be correctly accounted for in the radiative transfer and that in this case, the consistent mass-loss rates are obtained from the analysis of H$\alpha$ and the UV lines. These mass-loss rates are only factors 2-3 lower than the theoretical predictions (e.g. Mokiem et al. 2006). The new Monte-Carlo fully 3-D stellar wind models that account for the interclump medium confirm this result (Šurlan et al. 2012).

With all these in mind, we adopt $\dot{M} = 10^{-8} - 10^{-9}\,M_\odot\,\mathrm{yr}^{-1}$ and $v_\infty = 1000\,\mathrm{km\,s}^{-1}$ for the three O9.5V stars in sub-cluster 1. The other stars in NGC 602a are early B-type (or later) dwarfs, so their wind kinetic energies will be even smaller (see wind analysis of B-dwarfs in Oskinova et al. 2011). Thus, the combined input of kinetic energy from stellar winds in sub-cluster 1 is $L_{\rm mech} \lesssim 10^{33} - 10^{34}\,\mathrm{erg\,s}^{-1}$, which is too small to power the detected extended X-ray emission. This conclusion is supported by the morphology of the extended X-ray emission. Typically, WBBs have limb-brightened morphologies, where the diffuse X-ray emission is encompassed by, e.g., H$\alpha$ shells (Chu & Mac Low 1990; Toalá et al. 2012), but no such shell is seen around sub-cluster 1 (e.g., Fig. 2).

Beyond these considerations, we are unable to firmly exclude a contribution to the extended emission in sub-cluster 1 from a WBB. This is because, as noted in Section 2.2.1, the quality of the X-ray spectrum does not allow us to test multi-temperature spectral fits (Fig. 6). Also, we note that the experience from X-ray observations in the ONC suggests that *Chandra* is not ideally suited for detection of WBBs because of its rather low sensitivity for soft X-rays. The diffuse, hot ($T \sim 2$ MK) plasma discovered in the ONC by Güdel et al. (2008) was from *XMM-Newton* observations, and was not detected by *Chandra* (Feigelson et al. 2005). In part this was due to lower sensitivity of *Chandra* to soft X-rays. Moreover, the ONC is absorbed by a 'veil' of neutral gas (O'Dell et al. 2011) which was evident in the $N_{\rm H}$ measurements from *Chandra*; in the region further out where the diffuse emission was observed by *XMM-Newton*, the H I column density is much smaller.

Lastly, we also note that Güdel et al. (2008) explained all of the hard, extended X-ray emission observed in the ONC as being due to PMS stars. Arthur (2012) has recently presented hydrodynamic models for the expansion of WBBs inside evolving H II regions, adopting stellar wind parameters and a rate of ionizing photons appropriate to $\theta^1$ Ori C. She found that the model over-predicts the emission at higher energies compared to the observations. New physical ingredients (e.g., mass-loading, non-spherical models) may be required to reconcile WBB models for Orion with the observations. Thus, to firmly test a WBB model for NGC 602a we require dedicated theoretical models to arrive at robust predictions about their X-ray emission.

### 4.2. *Sub-cluster 1: X-ray Emission from pre-Main Sequence Stars*

X-ray observations of Galactic star-forming regions have revealed that *essentially all* low- and solar-mass PMS stars are X-ray sources. For example, *Chandra* observations of the ONC detected 98.5% of

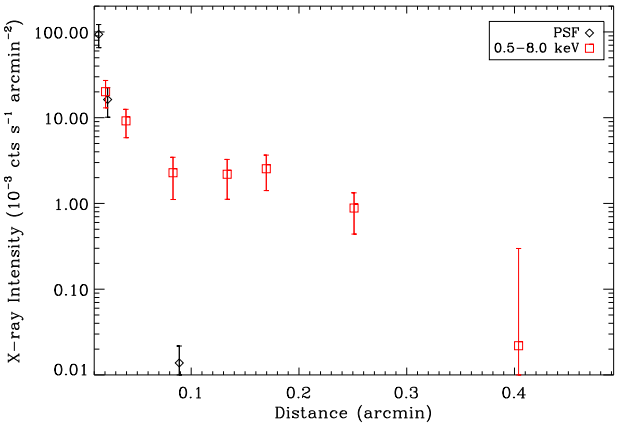


**Figure 5.** Radial profile of the extended X-ray emission in sub-cluster 1 of NGC 602a. The center is at $\alpha = 01^{\rm h}29^{\rm m}31^{\rm s}.104$, $\delta = -73^\circ33'44''.19$. The data points (red squares) represent bins with a signal-to-noise ratio $\geq 2.5$, with the exception of the last point. For comparison, the PSF of a point source (Source 4 from Table 1) in NGC 602a is shown (black squares).

the PMS stars known from optical and IR studies (Preibisch & Feigelson 2005). Thus, sufficiently deep X-ray observations of star clusters should be sensitive to the PMS population and the numerous (but individually faint) sources spread over a cluster may dominate the extended X-ray emission. This is especially true in a young clusters before the first supernovae and when the input of kinetic energy from massive stars is low due to their relative youth (e.g. Oskinova 2005) – sub-cluster 1 in NGC 602a is at such evolutionary stage.

There is a rich population of PMS stars in NGC 602a (Carlson et al. 2007; Schmalzl et al. 2008). Carlson et al. (2011) commented that low-mass PMS stars (with $0.6 < M < 3\,M_\odot$) were the most remarkable feature in the optical color-magnitude diagram of NGC 602a, with ages of generally less than $\sim$5 Myr. While some clumps of the PMS stars appear in the dusty outskirts of the cluster, the majority are concentrated in sub-cluster 1 (with an excess of 1 000 observed stars, Gouliermis et al. 2012).

We still know little about activity and accretion onto lower mass PMS stars in a low metallicty environment such as the SMC with except that their H$\alpha$ emission properties appear to be relatively normal (De Marchi et al. 2011). We hypothesize that the properties of PMS stars in NGC 602a are similar to those in the ONC. To test this hypothesis, we check whether we can explain the observed extended X-ray emission by *assuming* that stars of similar mass and age have the same X-ray properties in the ONC and NGC 602a.

The *Chandra* observations of the ONC allowed Preibisch & Feigelson (2005) to obtain X-ray luminosities of stars in different mass bins. They found that for PMS stars with ages in the range $\sim 0.1 - 10$ Myr stellar activity decays only mildly with age. We employ their statistical correlations (from their Table 1) between stellar mass, age, and X-ray luminosity in the 0.5-8 keV band and in four mass bins, namely: $0.1-0.2$, $0.2-0.4$, $0.4-1$, and $1-2\,M_\odot$.

For simplicity, we assume that all PMS stars in NGC 602a are coeval with ages of 4 Myr. At this age, intermediate mass stars ($2-8\,M_\odot$), would normally be recognized as a Herbig-type objects. Because HAeBe stars are not expected to possess an outer convective layer, X-ray emission detected from these objects is often attributed to low-mass companions. There is however evidence to suggest that in at least some HAeBe stars intrinsic X-ray emission can originate from solar-like magnetic coronae or magnetically confined winds or shock heated plasma in the jet or wind (Telleschi et al. 2007; Günther & Schmitt 2009). Whatever the origin of X-ray emission from intermediate mass young stars is, their X-ray luminosity is moderate, not exceeding a few$\times 10^{29}$ erg s$^{-1}$. Therefore, we assume that these stars are X-ray dim, and that their X-ray luminosity can be attributed to the less massive companion in binaries (e.g. Evans et al. 2011).

We assume a standard broken power law form for the IMF (Kroupa 2001) and randomly sample stars with masses between 0.1 $M_\odot$ and 50 $M_\odot$ (similar to the mass range for which Carlson et al. (2011) estimated the mass of the cluster) from this IMF. The results are not very sensitive to the high-mass cutoff used due to the small number of stars in these bins For a cluster mass of $\approx$ 2250 $M_\odot$, the number of stars between 0.1 $M_\odot$ and 2 $M_\odot$ is $\approx$ 3400. Their cumulative X-ray luminosity is $L_{\rm X} \approx 2.3 \times 10^{33}$ erg s$^{-1}$.

To check how sensitive the X-ray luminosity is to the cluster mass, we also considered a lower limit of $\approx$ 1600 $M_\odot$ for the total cluster mass as found by Cignoni et al. (2009) from optical data alone. In this case, the number of stars between 0.1 $M_\odot$ and 2 $M_\odot$ is $\approx$ 2500, and the total X-ray luminosity is $L_{\rm X} \approx 1.7 \times 10^{33}$ erg s$^{-1}$.

The cluster mass reported by Carlson et al. (2011) and Cignoni et al. (2009) is for the whole of NGC 602a. Based on the results of Gouliermis et al. (2012) we might expect the mass of sub-cluster 1, and hence the number of stars in this region, to be $\approx$ 25% smaller, so the above numbers would need to be scaled down accordingly.

With these assumptions, the model X-ray luminosity of PMS stars in NGC 602a is $L_{\rm X} \lesssim 2 \times 10^{33}$ erg s$^{-1}$ (0.5-8 keV band), in excellent agreement with the result from the spectral fits of the extended emission from sub-cluster 1 (see Section 2.2.1).

The spectral shape of extended X-ray emission from sub-cluster 1 also agrees well with the global X-ray properties of the low-mass population associated with the ONC from Feigelson et al. (2005). They found that a composite spectrum of low-mass stars in the ONC can be well represented by a two-temperature spectral model with $kT_1 = 0.5$ keV and $kT_2 = 3.3$ keV (with non-solar abundances), in modest agreement with those from the spectral fits in Section 2.2.1.

Thus, we believe that the extended X-ray emission is explained as originating from the unresolved population of low-mass, X-ray active PMS stars.

### 4.3. *Sub-cluster 2: X-ray emission from embedded class I YSOs*

The extended X-ray emission is also detected from the second most populous sub-cluster (see Section 2.2.2). We attribute this emission to the unresolved population of Class I YSOs.

Despite the large column densities in Galactic star-

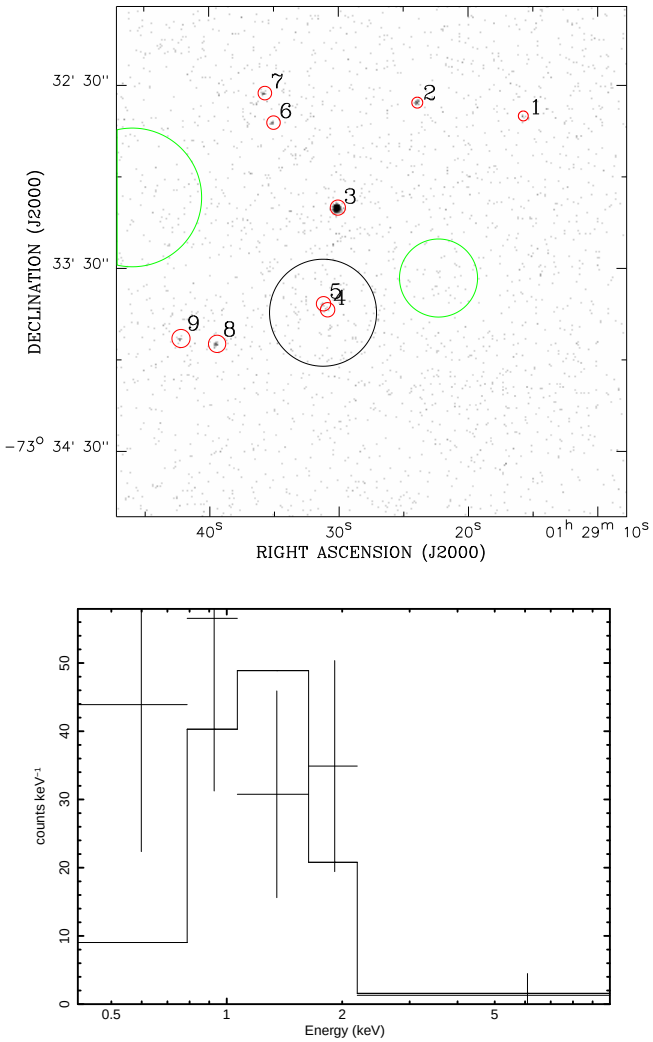


**Figure 6.** *Upper panel:* ACIS-I raw event map with the spectral extraction regions shown. Red circles: X-ray point sources; black circle: the region extracted to investigate the extended emission associated with sub-cluster 1 from Gouliermis et al. (2012); green circles: the regions used to extract background spectra. *Lower panel:* The spectrum of extended emission from sub-cluster 1 and its best fit isothermal (APEC) plasma model (see Section 2.2.1 for the model parameters). The spectrum is grouped such that the signal-to-noise ratio S/N = 2 in each energy bin. The best-fit model is found using Cash-statistics based fitting.

forming regions, Class I YSOs are routinely detected in X-rays, with typical luminosities of $L_{\rm X} \lesssim 10^{30}\,{\rm erg\,s^{-1}}$ (e.g. Getman et al. 2002; Preibisch & Feigelson 2005) and $L_{\rm X} \approx 10^{-4}\,L_{\rm bol}$ (e.g. Winston et al. 2010). Magnetic effects as well as accretion and jets are the likely key mechanisms responsible for X-ray production (Forbrich & Preibisch 2007).

The most energetic YSO at the tip of the "Pillar of Creation" in the Eagle Nebula has $L_{\rm X} \approx 3\times 10^{31}\,{\rm erg\,s^{-1}}$ (e.g. Guarcello et al. 2012), so dozens of such energetic YSOs would be needed to explain the X-ray luminosity of sub-cluster 2. Given that sub-cluster 2 is embedded in the dusty ridge, the absorption of X-rays will depend on the abundances and dust properties of that material (Wilms et al. 2000; Gordon et al. 2003), thus the estimates of the luminosity may be affected by the adopted extinction. An alternative explanation may involve true diffuse X-ray emission, e.g. as was suggested by Oskinova et al. (2010) who reported hard, diffuse X-rays from the Galactic star-forming region ON 2. Nevertheless, despite the large uncertainty in the estimated X-ray luminosity, one of the key results from the *Chandra* observations is the first X-ray detection of an embedded cluster of YSOs in the SMC.

## 5. DISCUSSION

X-ray observations of star-forming regions in the Galaxy have provided us with a high-energy perspective on stellar nurseries via studies of both individual stars and their overall stellar populations. The *Chandra* observations in the Wing of the SMC presented here allowed to obtain a high-energy view of a star-forming region in a very different environment. In addition to detections of point sources, the new observations have revealed extended X-ray emission emanating from the two most populous sub-clusters in NGC 602a.

Optical and IR observations of NGC 602a have shown that the basic properties of its low-mass stellar population do not appear significantly different to those in Galactic clusters with comparable mass and age. The continued star formation in the broken ring around NGC 602a is also analogous to regions seen in the Galaxy, which are often considered as an indication of a triggered second generations of star formation (e.g. Koenig et al. 2012).

Observations of the gas in the N 90 H II region demonstrated it to be nearly quiescent (Nigra et al. 2008), suggesting that there has not yet been a supernova explosion in the cluster[16]. A supernova remnant recently discovered at ∼110 pc to the west of NGC 602a (Hénault-Brunet et al. 2012) is most likely not related to this cluster, but rather to the general massive star population in the SMC's Wing. Stellar winds can therefore be expected to be the principal source of kinetic energy input into the intracluster medium, but at a reduced level compared to Galactic stars due to the weaker winds at the low metallicity of the SMC. In this context it's notable that the most massive star (Sk 183) is not detected in X-rays, in keeping with its low mass-loss rate (Evans et al. 2012). As might be expected for the low stellar wind efficiency calculated in Section 4.1, we do not see compelling evidence for a hot, diffuse gas filling the full cluster volume and originating from a cluster wind or a WBB. In this scenario, photo-ionization (which is dominated by Sk 183) is the primary driving mechanism in the evolution of the H II region N 90 (as discussed by Carlson et al. 2011, from different arguments).

We therefore suggest that the extended X-ray emission arises from the unresolved population of low-mass PMS stars (Section 4.2). As no individual PMS star (nor any flaring) is detected, this conclusion is based on the assumption that the coronal properties of the PMS stars in NGC 602a are comparable to the well-studied PMS stars in the ONC. Adopting the X-ray luminosities from PMS

[16] The non-thermal radio source in the vicinity of NGC 602a discussed by Nigra et al. as a possible supernova remnant is now identified with QSO J012930-733311

stars in the ONC we calculated an expected X-ray luminosity for sub-cluster 1 (on the basis of the known population of PMS stars). The predicted luminosity matches the luminosity of the extended emission obtained from our observations.

X-ray emission from PMS stars uniquely traces their *magnetic* activity, and provides an empirical foundation to the theory of magnetic dynamos – one of the key ingredient in stellar physics. We speculate that if the X-ray properties of PMS stars are indeed comparable in different environments, then other related properties, such as the formation and evolution of protoplanetary disks, are also likely to be similar.

The detection of hard X-ray emission from the YSOs residing at the tip of the 'elephant trunk' (sub-cluster 2) is also significant. Only 22 counts were detected (with no spectral or temporal information) but, in combination with the insights obtained from IR studies, such a detection suggests that the X-ray behaviour for the accretion and magnetospheric interactions in YSOs in the SMC arise from a similar mechanism to that in the Galaxy.

This study is based on observations obtained by the *Chandra* science mission, and spectroscopy obtained from ESO program 086.D-0167. This study used software provided by the *Chandra* CXC, and made use of the NASA Astrophysics Data System Service and the SIMBAD database. We thank D. Gouliermis for providing us with the maps of stellar density in NGC 602a. The authors thank Jacco Vink, Leisa K. Townsley, and Helge Todt for useful discussions. We also thank the referee for useful and detailed comments which led to considerable improvement of the manuscript. Support is acknowledged as follows – LMO: DLR grant 50 OR 1101; VHB: SUPA and NSERC; YN: FNRS, CFWB, ARC, and PRODEX; CJE: Caledonian 80/-; MAG: MICINN grant AYA2011-29754-C03-02, which includes FEDER funds; WS: DAAD grant A/10/95420; WS and YC: NSFC grant 11233001 and 973 Program grant 2009CB824800; SS: Conacyt research grant 131913; YHC, JSG, and RAG: NASA grants SAO GO0-11025X and NNX11AH96G. JSG also thanks donors to the University of Wisconsin-Madison College of Letters & Science for partial support of this research.

## APPENDIX

## A. COUNTERPARTS TO DETECTED X-RAY POINT SOURCES IN NGC 602A

The positions of the nine point sources detected in the *Chandra* observations are overlaid on the optical *HST* image shown in Fig. 2. As noted in Section 2.1, source 2 lacks a convincing optical counterpart, we now discuss the other eight in turn.

### A.1. *Sources 1 and 8*

Sources 1 and 8 have faint optical counterparts. Source 1 is 1.″6 away from SGD 3373 (25.6 mag. in F555W filter; Schmalzl et al. 2008). Source 8 coincides with SGD 3012 (26.8 mag. in F555W filter; Schmalzl et al. 2008). We assume that these objects are background AGNs.

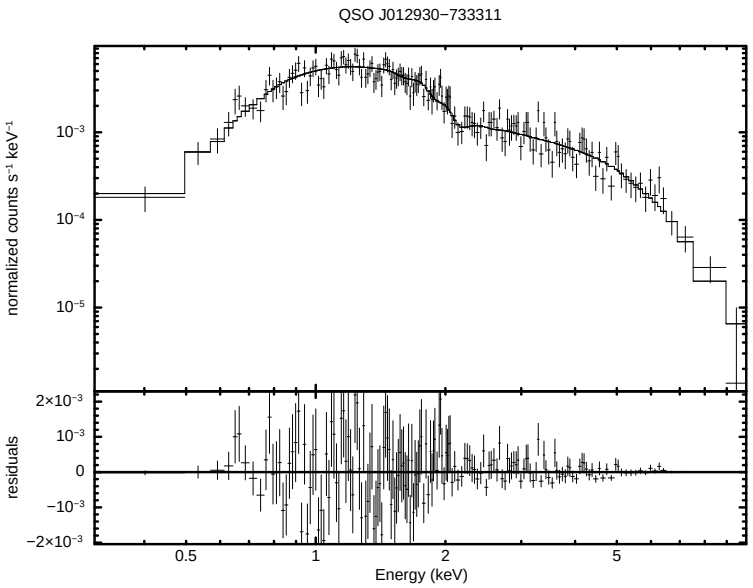


**Figure 7.** *Upper panel*: the *Chandra* ACIS-I spectrum of QSO J012930-733311 with the best-fitting absorbed power-law model (solid lines, see Section A.2); *Lower panel:* residuals between the model and the observed spectrum.

### A.2. *Source 3 QSO J012930-733311 and the neutral hydrogen absorption estimates*

Source 3 is the most luminous X-ray object in NGC 602a, and corresponds to the candidate YSO from Gouliermis et al. (2007, their source 52) and Carlson et al. (2011, their Y283). FLAMES spectroscopy revealed this source to be a quasar (QSO) at a redsfhit of $z = 2.438 \pm 0.003$ (labelled as 'QSO' in Fig. 2). Following the IAU recommendations on nomenclature we designate this as QSO J012930-733311 ($\alpha = 01^{\rm h}\,29^{\rm m}\,30\overset{\rm s}{.}17$; $\delta = -73^\circ\,33'\,10\overset{''}{.}77$; J2000). The X-ray spectrum of the QSO can be well fitted by an absorbed power-law model with $\Gamma \approx 1.8$, and its observed flux is $1.1 \times 10^{-13}\,{\rm erg\,s^{-1}\,cm^{-2}}$. Its spectrum and the best-fit model are shown in Fig. 7.

To model the absorbing column of gas towards QSO J012930-733311 we used two components to account for Galactic and local SMC absorption. The X-ray spectrum of QSO J012930-733311 does not show apparent signs of the intrinsic absorption by the QSO, as well as any cosmological absorption (e.g., Behar et al. 2011), so these components were ignored. Assuming solar abundances, the Galactic foreground absorption was fixed at a column density of $6 \times 10^{20}\,{\rm cm^{-2}}$ (Wilms et al. 2000). A second component (with SMC abundances) was fitted, yielding a value of $(2.0 \pm 0.4) \times 10^{21}\,{\rm cm^{-2}}$.

This value compares well with the SMC neutral hydrogen density toward NGC 602a of $(2.0 - 2.5) \times 10^{21}\,{\rm cm^{-2}}$ from the radio maps from Stanimirovic et al. (1999), which are sensitive to all angular (spatial) scales between 98″ (26 pc) and 4° (4 kpc).

The reddening toward Sk 183 was estimated by Evans et al. (2012) to be $E(B-V) = 0.09$ mag. This corresponds to $\approx 4 \times 10^{21}\,{\rm cm^{-2}}$ (Bouchet et al. 1985).

We therefore have at least three independent estimates – in good agreement – of the absorbing column towards NGC 602a, i.e., from fits to the X-ray spectrum of QSO J012930-733311, from the H I maps of the SMC

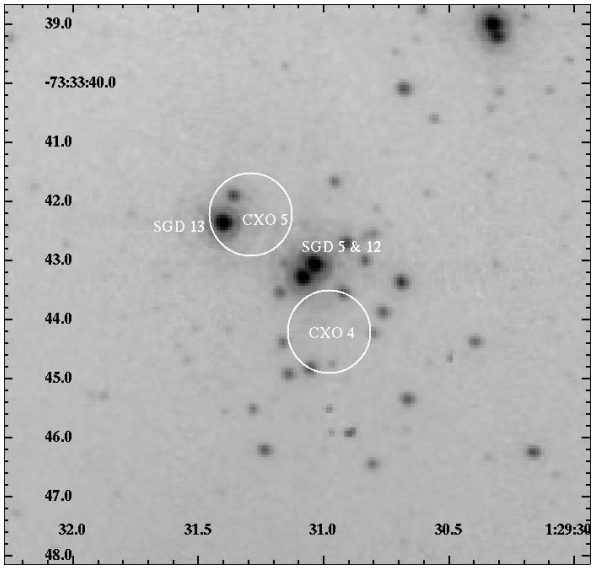


**Figure 8.** *HST* F658N image of the central $\sim 10'' \times 10''$ (2.6 pc × 2.6 pc) of NGC 602a. Bright OB-type stars are labelled with identifications from Schmalzl et al. (2008, SGD). Point sources detected in the *Chandra* observations (see Table 1) are shown by the white circles (with a radius of $0\farcs7$).

(Stanimirovic et al. 1999), and from optical photometry/spectroscopy of the massive stars in the cluster.

### A.3. *Source 4*

Source 4 is $1\farcs04$ ($\sim 0.3$ pc) from star HTCP 2 (Hutchings et al. 1991), which they classified as O9. HTCP 2 was later resolved into a close pair of stars by the *HST* imaging (see Fig. 8): SGD 5 and 12, with 15.371 mag. and 15.816 mag. in the F555W filter respectively (Schmalzl et al. 2008). The FLAMES–Medusa fibers subtend $1\farcs2$ on the sky, so our spectroscopy of HTCP 2 will include contributions from both SGD 5 and 12. Within the separate spectra we saw no qualitative evidence for radial velocity shifts, and the combined spectrum was classified as O9.5 V. The astrometric uncertainty on the position of the X-ray source is $0\farcs5$ (see Table 1), thus we can not securely identify SGD 5 and/or 12 as counterparts. Nevertheless, we note that source 4 has a modest X-ray count rate and is detected in a soft band, which would be expected from a normal OB-type star.

### A.4. *Source 5*

There are two sources within the astrometric uncertainty of the X-ray position for source 5 (see Fig. 8). Both potential counterparts have photometry from Schmalzl et al. (2008): SGD 13 has 15.663 mag. in F555W filter and 15.871 mag. in F814W filter; SGD 119 has 19.201 mag. in F555W filter and 19.228 mag. in F814W filter. We have an optical spectrum of SGD 13 from FLAMES, but it was only observed with the Giraffe LR02 setting (covering $\lambda\lambda$3960-4564 Å). We provisionally classify the spectrum as O9.5: V, but note that we lack full coverage of the optical region usually employed for classification of massive stars. Although SGD 13 and 119 are only separated by $\sim 0\farcs5$, their relative magnitudes mean that SGD 13 should dominate the spectrum.

To investigate the nature of the fainter source, we take the *HST* filters as approximately $V$- and $I$-bands, and adopt the intrinsic colour for an O9.5 dwarf from Johnson (1966) and extinction relations from Howarth (1983). The approximate line-of-sight reddening toward SGD 13 from these assumptions is $E(B-V) \approx 0.16$ mag. Adopting the same reddening for SGD 119 to estimate its absolute magnitude and intrinsic colour suggests it as a mid-late B-type dwarf. We note that if SGD 119 were a magnetic B-type star, it is unlikely that its X-ray luminosity would be as large as that detected for source 5 (cf. Oskinova et al. 2011).

Provided SGD 119 is not a background source, SGD 13 seems the most likely counterpart, but given the limited wavelength coverage of the FLAMES spectrum it is hard to speculate further on its nature at this point. If SGD 13 were the genuine counterpart, its X-ray luminosity ($L_{\rm X} = 3 \pm 1 \times 10^{32}\,{\rm erg\,s^{-1}}$) would correspond to $\log L_{\rm X}/L_{\rm bol} \lesssim -6.3$. Following the same arguments as in Section 3, a colliding-wind system could account for the larger-than-expected X-ray luminosity. Equally, the object could be analogous to the X-ray variable system $\theta^2$ Ori A, which has a quiescent X-ray luminosity of $\sim 8 \times 10^{31}\,{\rm erg\,s^{-1}}$ (D. Huenemoerder, private communication), with its behaviour suggested by Mitschang et al. (2011) as comparable to what would be expected from a magnetically-confined wind model.

### A.5. *Source 6*

Source 6 is coincident with the candidate YSO 'Y358' from Carlson et al. (2011). At the distance of NGC 602a, its X-ray luminosity would be $L_{\rm X} \approx 6 \times 10^{32}\,{\rm erg\,s^{-1}}$, which is rather high for a low-mass YSO. The optical magnitudes of Y358 are too faint for it to be a young massive star in this region of relatively low extinction (22.695 mag. in F555W filter and 21.970 mag. in F814W filter Schmalzl et al. 2008). Given its relative isolation, we suggest that source 6 is a background object rather than a genuine YSO.

### A.6. *Source 7*

Source 7 coincides with a spiral galaxy ('G372' from Carlson et al. 2011), which can be seen clearly in the *HST* image (Fig. 2).

### A.7. *Source 9*

Source 9 is $\approx 1\farcs6$ away from an optical source SGD 3593 (F555W = 25.892 mag. and F814W = 24.809 mag. Schmalzl et al. 2008). Visual inspection of the *HST* ACS images shows that the optical object is fuzzy and strongly resembles a galaxy. We thus believe that *Chandra* source 9 is a background galaxy.

## REFERENCES

Adams, F. C., Lada, C. J., & Shu, F. H. 1987, ApJ, 312, 788
Alves, J., & Bouy, H. 2012, A&A, 547, A97
Antokhin, I. I., Owocki, S. P., & Brown, J. C. 2004, ApJ, 611, 434
Arnaud, K. A. 1996, in Astronomical Society of the Pacific Conference Series, Vol. 101, Astronomical Data Analysis Software and Systems V, ed. G. H. Jacoby & J. Barnes, 17
Arthur, S. J. 2012, MNRAS, 421, 1283
Babel, J., & Montmerle, T. 1997, ApJ, 485, L29
Behar, E., Dado, S., Dar, A., & Laor, A. 2011, ApJ, 734, 26
Berghoefer, T. W., Schmitt, J. H. M. M., Danner, R., & Cassinelli, J. P. 1997, A&A, 322, 167

Bouchet, P., Lequeux, J., Maurice, E., Prevot, L., & Prevot-Burnichon, M. L. 1985, A&A, 149, 330
Bouret, J.-C., Lanz, T., Hillier, D. J., et al. 2003, ApJ, 595, 1182
Caramazza, M., Micela, G., Prisinzano, L., et al. 2012, A&A, 539, A74
Carlson, L. R., Sabbi, E., Sirianni, M., et al. 2007, ApJ, 665, L109
Carlson, L. R., Sewiło, M., Meixner, M., et al. 2011, ApJ, 730, 78
Cerviño, M., & Valls-Gabaud, D. 2003, MNRAS, 338, 481
Chabrier, G. 2003, PASP, 115, 763
Chini, R., Hoffmeister, V. H., Nasseri, A., Stahl, O., & Zinnecker, H. 2012, MNRAS, 424, 1925
Chu, Y.-H., & Mac Low, M.-M. 1990, ApJ, 365, 510
Cignoni, M., Sabbi, E., Nota, A., et al. 2009, AJ, 137, 3668
De Marchi, G., Panagia, N., & Sabbi, E. 2011, ApJ, 740, 10
Donati, J.-F., Babel, J., Harries, T. J., et al. 2002, MNRAS, 333, 55
Drake, S. A., Linsky, J. L., Schmitt, J. H. M. M., & Rosso, C. 1994, ApJ, 420, 387
Evans, C. J., Hainich, R., Oskinova, L. M., et al. 2012, ApJ, 753, 173
Evans, N. R., DeGioia-Eastwood, K., Gagné, M., et al. 2011, ApJS, 194, 13
Feigelson, E. D., Broos, P., Gaffney, III, J. A., et al. 2002, ApJ, 574, 258
Feigelson, E. D., Getman, K., Townsley, L., et al. 2005, ApJS, 160, 379
Flaccomio, E., Damiani, F., Micela, G., et al. 2003, ApJ, 582, 398
Forbrich, J., & Preibisch, T. 2007, A&A, 475, 959
Gagné, M., Oksala, M. E., Cohen, D. H., et al. 2005, ApJ, 628, 986
Gallagher, III, J. S., & Hunter, D. A. 1984, ARA&A, 22, 37
Getman, K. V., Feigelson, E. D., Townsley, L., et al. 2002, ApJ, 575, 354
Getman, K. V., Flaccomio, E., Broos, P. S., et al. 2005, ApJS, 160, 319
Gordon, K. D., Clayton, G. C., Misselt, K. A., Landolt, A. U., & Wolff, M. J. 2003, ApJ, 594, 279
Gouliermis, D. A., Quanz, S. P., & Henning, T. 2007, ApJ, 665, 306
Gouliermis, D. A., Schmeja, S., Dolphin, A. E., et al. 2012, ApJ, 748, 64
Gräfener, G., & Hamann, W.-R. 2008, A&A, 482, 945
Guarcello, M. G., Caramazza, M., Micela, G., et al. 2012, ApJ, 753, 117
Güdel, M., Briggs, K. R., Montmerle, T., et al. 2008, Science, 319, 309
Günther, H. M., & Schmitt, J. H. M. M. 2009, A&A, 494, 1041
Hénault-Brunet, V., Oskinova, L. M., Guerrero, M. A., et al. 2012, MNRAS, 420, L13
Henize, K. G. 1956, ApJS, 2, 315
Hillenbrand, L. A. 1997, AJ, 113, 1733
Hillenbrand, L. A., & Hartmann, L. W. 1998, ApJ, 492, 540
Howarth, I. D. 1983, MNRAS, 203, 801
Huenemoerder, D. P., Oskinova, L. M., Ignace, R., et al. 2012, ApJ, 756, L34
Hutchings, J. B., Cartledge, S., Pazder, J., & Thompson, I. B. 1991, AJ, 101, 933
Ignace, R., Oskinova, L. M., & Massa, D. 2012, MNRAS, 288
Jerius, D., Donnelly, R. H., Tibbetts, M. S., et al. 2000, in Society of Photo-Optical Instrumentation Engineers (SPIE) Conference Series, Vol. 4012, Society of Photo-Optical Instrumentation Engineers (SPIE) Conference Series, ed. J. E. Truemper & B. Aschenbach, 17–27
Johnson, H. L. 1966, ARA&A, 4, 193
Koenig, X. P., Leisawitz, D. T., Benford, D. J., et al. 2012, ApJ, 744, 130
Kroupa, P. 2001, MNRAS, 322, 231
Lee, J.-K., Rolleston, W. R. J., Dufton, P. L., & Ryans, R. S. I. 2005, A&A, 429, 1025
Liu, Q. Z., van Paradijs, J., & van den Heuvel, E. P. J. 2005, A&A, 442, 1135
Martins, F., Schaerer, D., Hillier, D. J., & Heydari-Malayeri, M. 2004, A&A, 420, 1087
Massey, P., Lang, C. C., Degioia-Eastwood, K., & Garmany, C. D. 1995, ApJ, 438, 188
Meaburn, J. 1980, MNRAS, 192, 365
Mitschang, A. W., Schulz, N. S., Huenemoerder, D. P., Nichols, J. S., & Testa, P. 2011, ApJ, 734, 14
Mokiem, M. R., de Koter, A., Evans, C. J., et al. 2006, A&A, 456, 1131
Mokiem, M. R., de Koter, A., Vink, J. S., et al. 2007, A&A, 473, 603
Nazé, Y. 2009, A&A, 506, 1055
Nazé, Y., Hartwell, J. M., Stevens, I. R., et al. 2003, ApJ, 586, 983
Nazé, Y., Mahy, L., Damerdji, Y., et al. 2012, A&A, 546, A37
Nazé, Y., Broos, P. S., Oskinova, L., et al. 2011, ApJS, 194, 7
Nigra, L., Gallagher, III, J. S., Smith, L. J., et al. 2008, PASP, 120, 972
O'Dell, C. R., Ferland, G. J., Porter, R. L., & van Hoof, P. A. M. 2011, ApJ, 733, 9
Oskinova, L. M. 2005, MNRAS, 361, 679
Oskinova, L. M., Clarke, D., & Pollock, A. M. T. 2001, A&A, 378, L21
Oskinova, L. M., Gruendl, R. A., Ignace, R., et al. 2010, ApJ, 712, 763
Oskinova, L. M., Hamann, W.-R., & Feldmeier, A. 2007, A&A, 476, 1331
Oskinova, L. M., Todt, H., Ignace, R., et al. 2011, MNRAS, 416, 1456
Pallavicini, R., Golub, L., Rosner, R., et al. 1981, ApJ, 248, 279
Pizzolato, N., Ventura, P., D'Antona, F., et al. 2001, A&A, 373, 597
Pollock, A. M. T., & Corcoran, M. F. 2006, A&A, 445, 1093
Preibisch, T., & Feigelson, E. D. 2005, ApJS, 160, 390
Puls, J., Kudritzki, R.-P., Herrero, A., et al. 1996, A&A, 305, 171
Sabbi, E., Sirianni, M., Nota, A., et al. 2008, AJ, 135, 173
Sana, H., de Mink, S. E., de Koter, A., et al. 2012, Science, 337, 444
Sandstrom, K. M., Peek, J. E. G., Bower, G. C., Bolatto, A. D., & Plambeck, R. L. 2007, ApJ, 667, 1161
Schmalzl, M., Gouliermis, D. A., Dolphin, A. E., & Henning, T. 2008, ApJ, 681, 290
Schulz, N. S., Canizares, C., Huenemoerder, D., et al. 2001, ApJ, 549, 441
Seward, F. D., Forman, W. R., Giacconi, R., et al. 1979, ApJ, 234, L55
Silich, S., Tenorio-Tagle, G., & Añorve-Zeferino, G. A. 2005, ApJ, 635, 1116
Smith, B. J., Struck, C., & Nowak, M. A. 2005, AJ, 129, 1350
Stanimirovic, S., Staveley-Smith, L., Dickey, J. M., Sault, R. J., & Snowden, S. L. 1999, MNRAS, 302, 417
Stevens, I. R., Blondin, J. M., & Pollock, A. M. T. 1992, ApJ, 386, 265
Stevens, I. R., & Hartwell, J. M. 2003, MNRAS, 339, 280
Telleschi, A., Güdel, M., Briggs, K. R., et al. 2007, A&A, 468, 541
Toalá, J. A., Guerrero, M. A., Chu, Y.-H., et al. 2012, ApJ, 755, 77
Townsley, L. K., Feigelson, E. D., Montmerle, T., et al. 2003, ApJ, 593, 874
Townsley, L. K., Broos, P. S., Corcoran, M. F., et al. 2011, ApJS, 194, 1
Šurlan, B., Hamann, W.-R., Kubát, J., Oskinova, L. M., & Feldmeier, A. 2012, A&A, 541, A37
Vink, J. S., de Koter, A., & Lamers, H. J. G. L. M. 2001, A&A, 369, 574
Wang, Q. D. 2004, ApJ, 612, 159
Westerlund, B. E. 1964, MNRAS, 127, 429
Wilms, J., Allen, A., & McCray, R. 2000, ApJ, 542, 914
Winston, E., Megeath, S. T., Wolk, S. J., et al. 2010, AJ, 140, 266
Yasui, C., Kobayashi, N., Tokunaga, A. T., Saito, M., & Tokoku, C. 2009, ApJ, 705, 54